JGP Journal of General Physiology

ARTICLE

Regulation of NMDAR activation efficiency by environmental factors and subunit composition

Miaomiao He[1,3,4] and Lonnie P. Wollmuth[2,3,4]

NMDA receptors (NMDAR) convert the major excitatory neurotransmitter glutamate into a synaptic signal. A key question is how efficiently the ion channel opens in response to the rapid exposure to presynaptic glutamate release. Here, we applied glutamate to single channel outside-out patches and measured the successes of channel openings and the latency to first opening to assay the activation efficiency of NMDARs under different physiological conditions and with different human subunit compositions. For GluN1/GluN2A receptors, we find that various factors, including intracellular ATP and GTP, can enhance the efficiency of activation presumably via the intracellular C-terminal domain. Notably, an energy-based internal solution or increasing the time between applications to increase recovery time improved efficiency. However, even under these optimized conditions and with a 1-s glutamate application, there remained around 10–15% inefficiency. Channel activation became more inefficient with brief synaptic-like pulses of glutamate at 2 ms. Of the different NMDAR subunit compositions, GluN2B-containing NMDARs showed the lowest success rate and longest latency to first openings, highlighting that they display the most distinct activation mechanism. In contrast, putative triheteromeric GluN1/GluN2A/GluN2B receptors showed high activation efficiency. Despite the low open probability, NMDARs containing either GluN2C or GluN2D subunits displayed high activation efficiency, nearly comparable with that for GluN2A-containing receptors. These results highlight that activation efficiency in NMDARs can be regulated by environmental surroundings and varies across different subunits.

Introduction

Among the diverse neurotransmitters, glutamate is notable for its prominence in mediating a broad spectrum of brain activity, including excitatory neurotransmission and the plasticity that underlies learning and memory (Watkins and Jane, 2006; Herring and Nicoll, 2016; Hansen et al., 2021). Ionotropic glutamate receptors (iGluRs) are tetrameric ligand-gated ion channels activated by the neurotransmitter glutamate and permeable to the monovalent cations K^+ and Na^+, as well as the divalent Ca^{2+}. At synapses, their essential function involves triggering rapid synaptic excitation and multiple Ca^{2+}-associated intracellular events (Paoletti et al., 2013; Hansen et al., 2021). Improper signaling by iGluRs is associated with neurological, neurodevelopmental, and psychiatric disorders including stroke, Parkinson's disease, epilepsy, intellectual disability, autism, and schizophrenia among others (Coyle, 2017; XiangWei et al., 2018; Choi, 2020; Wang et al., 2020; Prüss, 2021; Wollmuth et al., 2021).

The two major post-synaptic iGluRs are AMPA receptors (AMPAR) and NMDA receptors (NMDARs). In response to the transient glutamate arising from presynaptic release, these receptor subtypes exhibit different kinetic responses. In general, AMPARs activate rapidly (but see Pampaloni et al., 2021; Pampaloni and Plested, 2022), whereas NMDARs demonstrate a much slower and delayed kinetic component. A key question is how iGluRs activate in response to glutamate exposure since this directly impacts postsynaptic signaling. The question of activation efficiency is especially pertinent to the slow kinetics of NMDARs (Traynelis et al., 2010).

NMDARs are obligate heterotetramers formed by two glycine-binding GluN1 subunits and typically two glutamate-binding GluN2 (A-D) subunits (Traynelis et al., 2010; Karakas and Furukawa, 2014; Lee et al., 2014; Wang et al., 2021). The different GluN2 subunits can show a wide range of ion channel gating properties that contribute to their diverse roles in cell-to-cell signaling (Erreger et al., 2005; Dravid et al., 2008; Vance et al., 2011, 2013; Paoletti et al., 2013; Hansen et al., 2014; Glasgow et al., 2015; Bhattacharya et al., 2018).

To address activation efficiency in NMDARs, we recorded from outside-out patches containing a single NMDAR. We applied glutamate and assayed successes, whether the channel

[1]Graduate Program in Biochemistry and Structural Biology, Stony Brook University, Stony Brook, NY, USA; [2]Department of Neurobiology and Behavior, Stony Brook University, Stony Brook, NY, USA; [3]Department of Biochemistry and Cell Biology, Stony Brook University, Stony Brook, NY, USA; [4]Center for Nervous System Disorders, Stony Brook University, Stony Brook, NY, USA.

Correspondence to Lonnie P. Wollmuth: lonnie.wollmuth@stonybrook.edu.

opened or not, and if it opened the "latency to first opening," which is the time interval between the onset of glutamate application to the first detectable opening of the ion channel (Amin et al., 2021). This approach is advantageous to assay activation efficiency because aside from assuming near instantaneous binding of glutamate, it involves few assumptions about the kinetic process. The outcome of these experiments also has physiological implications since they highlight how efficiently channels will open in response to rapid presynaptically released glutamate.

Previously, we used solutions to assay the biophysical properties of NMDARs (Amin et al., 2021). These included using pH 8.0 to enhance gating and an internal solution that solely contained KCl, with no energy-based components. Despite trying to optimize channel opening, GluN1/GluN2A channels showed frequent failures. Considering the importance of the microenvironment in regulating NMDARs' activity (Hansen et al., 2021; Mony and Paoletti, 2023), we address how variations in external and internal solutions and different human GluN2 subunits alter NMDAR activation efficiency. We find that activation efficiency is regulated by environmental conditions, including energy-based internals and by GluN2 subunits. Notably, GluN2B-containing NMDARs display the most distinct activation mechanism. These experiments lay the foundation to further resolve the activation mechanisms of NMDARs and their contribution to fast synaptic transmission.

Materials and methods

Mutagenesis and expression

NMDAR constructs used include (NCBI Protein database accession no.) rat (P35439) and human (Q05586) GluN1 (GluN1-1a); rat (Q00959) and human (Q12879) GluN2A; human GluN2B (Q13224); human GluN2C (Q14957); and human GluN2D (O15399). All human constructs were provided by Dr. Stephen Traynelis and the Center for Functional Evaluation of Rare Variants (Emory University, Atlanta, GA, USA). The GluN1-1a splice variant was used in all instances.

We transiently co-transfected cDNA constructs of GluN1 and GluN2 subunits into mammalian human embryonic kidney 293 (HEK293) with a separate pEGFP-Cl vector (Clontech) at a ratio of 4.5:1:1 (GluN1/GluN2/eGFP) using X-tremeGENE HP (Roche) (Yelshansky et al., 2004; Amin et al., 2017). Cells were grown at 37°C and 5% CO_2 in Dulbecco's modified Eagle's medium containing 10% fetal bovine serum for 24 h before transfection. To increase cell viability via limiting Ca^{2+} influx, the media bathing transfected cells also contained the NMDAR competitive antagonist amino-5-phosphonovaleric acid (APV, 100 µM) and non-competitive antagonist Mg^{2+} (100 µM). Patch clamp recordings were performed 18–36 h after transfection.

Triheteromeric expression system

NMDARs are typically composed of 2 GluN1 and 2 GluN2 subunits. To restrict surface expression to defined triheteromeric receptors (i.e., GluN1/GluN2A/GluN2B), we used a "triheteromeric" system (Hansen et al., 2014), which is based on leucine zipper motifs from $GABA_B$ receptors (LZ1 and LZ2) and dilysine ER retention motifs (KKXX retention motif) introduced into the C-terminal domain of NMDAR subunits. Specifically, tetrameric assemblies containing just C1 (LZ1/ER retention motif) or C2 (LZ2/ER retention motif) alone do not dimerize and are retained in the ER. In contrast, in tetrameric assemblies containing both C1 and C2, the LZ1 and LZ2 motifs dimerize, which masks the ER retention motif, allowing surface expression. All constructs (pCI-neo-GluN2A-C1-L4, pCI-neo-GluN2A-C2-L4, pCI-neo-GluN2B-AC1-L4, and pCI-neo-GluN2B-AC2-L4) are based on rat sequences and were kindly provided by Dr. Kasper Hansen (University of Montana, Missoula, MT, USA).

Outside-out single-channel recordings

Outside-out single-channel recordings were collected at room temperature (21–24°C) using an EPC-10 patch clamp amplifier interfaced with PatchMaster (HEKA). We used thick-walled, borosilicate glass (Sutter Instrument) for patch pipettes, which were pulled and fire-polished yielding resistances between 5 and 20 MΩ when measured in the bath solution (with applied positive pressure of ∼150 mbar).

Patch pipettes contained either 140 mM KCl, 10 mM HEPES, and 1 mM 1,2-bis(o-aminophenoxy)ethane-N,N,N′,N′-tetraacetic acid (BAPTA) (pH 7.3, NaOH) (used in Amin et al., 2021) or 140 mM KCl, 2 mM NaCl, 10 mM HEPES, 4 mM Mg_2ATP, 0.3 mM GTP, and 1 mM BAPTA (pH 7.3, KOH). We refer to the latter solution, which contains free energy from ATP and GTP, as an "energy-based internal solution." Such an energy-based internal is a common internal solution when recording from brain slices (Watanabe et al., 2005; Helmstaedter et al., 2009; Ferrer et al., 2018).

In terms of external solutions, our standard external solution consists of (in mM): 150 NaCl, 10 HEPES, and 0.05 EDTA, pH 7.4 or 8.0 (NaOH). This solution at pH 8 was used in Amin et al. (2021) and removes the complications of proton (high pH 8.0) and divalent (Zn^{2+}) inhibitory effects (Popescu and Auerbach, 2003) and the short- (Maki and Popescu, 2014) and long- (Legendre et al., 1993) term effects of Ca^{2+} on NMDARs.

We applied 2-ms or 1-s pulses of 1 mM glutamate through a piezo-driven double-barrel application pipette system (10–90% rise time of 400–600 µs). The baseline barrel contained the Na-based external and 0.1 mM glycine while the test barrel contained the identical solution except for added 1 mM glutamate. For GluN1/GluN2A, the interval between the start of a pulse and the start of the next pulse was either 4 or 10 s to allow recovery from desensitization (tau of recovery from desensitization for wild-type GluN1/GluN2A is around 1 s (Alsaloum et al., 2016). For GluN1/GluN2B, the interval was 20 s. Currents were recorded at −60 mV.

The time course for glutamate in the synaptic cleft is roughly described by a peak of ∼1 mM that decays with a time constant of ∼1 ms (Clements et al., 1992). Under such a scenario, and assuming an EC_{50} for glutamate of 3 µM for GluN1/GluN2A or GluN1/GluN2B receptors (Traynelis et al., 2010), NMDARs would be exposed to saturating glutamate concentrations for ∼2–3 ms. We therefore used 2-ms glutamate pulses to mimic synaptic-like glutamate exposures.

Analysis of single-channel outside-out patches

We exposed outside-out patches to super-saturating concentrations of glutamate (1 mM) and glycine (100 µM) (Traynelis et al., 2010) to ensure receptor saturation and that the agonist binding steps occurred as rapidly as possible. For most of our experiments, we applied glutamate for 1 s, which allowed us to more readily determine whether patches contained just a single receptor, facilitating obtaining a high number of events. Brief agonist applications (e.g., 1–2 ms as occurs at synapses [Clements et al., 1992]) make it harder to determine the number of channels in the patch since many of the patches last for only 10–30 applications.

Given the high open probability and relatively long open time of GluN1-1a/GluN2A, we were quite confident that patches contained a single receptor; many patches were rejected because of two or more channels. In contrast, GluN2B-, GluN2C-, and GluN2D-containing receptors showed a much lower open probability and had briefer open times (Banke and Traynelis, 2003; Dravid et al., 2008; Vance et al., 2013). We were unable to carry out long recordings to carry out statistical tests (Dravid et al., 2008; Kazi et al., 2013) to verify that there was only a single channel. Hence, it is possible that these patches contained two channels, though we think it is unlikely.

To analyze outside-out patches, we exported data from PatchMaster (HEKA Elektronik) to Igor (Wavemetrics), where they were analyzed using in-house developed programs. Applications or sweeps displaying significant amounts of noise were removed (~5–10% of applications). Patches were included in the histogram analysis only if they included a minimum of 10 applications or trials (see below).

Latency to first opening

To assay NMDAR activation, we measured durations from the start of an application to the first open event (latency or latency to first opening) (Aldrich et al., 1983; Goldschen-Ohm et al., 2013; Amin et al., 2021). To define the start of the application, we assayed the rise time of the application pipette on going from 100% to 10% external solution during the day of experimentation. We defined the start of the glutamate application around the 10% rise time of this test application. In general, we found the rise time to be highly consistent with a specific application pipette.

To identify the first single-channel event, we used a threshold-crossing approach in code written in Igor Pro. To define a threshold, we started with the maximum (extrema) noise level in the baseline (often around −2 pA) for each individual sweep prior to the glutamate application and added a subunit-specific correction factor: −1 pA for GluN2A- and GluN2B- and −0.5 pA for GluN2C- and GluN2D-containing receptors. An inward current deflection was classified as a single channel event if it crossed this defined threshold. Although this algorithm was highly efficient at automatically detecting the first single-channel event, there were periodic small amplitude events that were clear noise, which were incorrectly detected. We therefore visually inspected each sweep to verify the accuracy of the detected event.

Latency to first opening times for a specific condition was pooled and imported into ChannelLab (Synaptosoft). Latencies were binned at ~60-µs intervals and histograms displaying the number of events as a function of latency to first opening were generated. We fit the cumulative histogram with one or multiple exponentials until the log-likelihood score could not be further improved. In almost all instances, the best fit was two exponentials, a fast and a slow component:

$$N_S(t) = N_{fast}\exp^{-t/\tau_{fast}} + N_{slow}\exp^{-t/\tau_{slow}}$$

where N_S is the number of successes, t is time, and N_{fast} and N_{slow} are the number of events classified as fast or slow, and τ_{fast} and τ_{slow} the fitted exponentials.

Failure to open

In some instances, agonist application showed no discernible NMDAR-mediated currents either during or after agonist removal (2 s total). These instances are referred to as failures. In the text, successes = 1 − failure rate. Because we included patches with a wide range of events in the success rate, which might bias the average value in one direction, we also indicate the "global success rate," which is the total number of successes for all patches divided by the total number of trials.

Efficiency (η) of activation

As noted above, it is extremely challenging to resolve single-channel patches using brief synaptic-like (1–2 ms) applications of glutamate. We therefore mainly used a 1-s application to aid in defining single-channel patches. On the other hand, while our focus was on quantifying the transition from the closed to the open state (latency to first opening), we also wanted to put these transitions in a physiological perspective in terms of what events might contribute to fast synaptic events. We therefore defined the efficiency (η) of activation as Amin et al. (2021):

$$efficiency\ (\eta) = \frac{(successes * fraction\ fast\ component)}{total\ number\ of\ trials\ (N_T)} = \frac{N_{fast}}{N_T}$$

In terms of 1-s glutamate applications, there are three general outcomes: (1) fast and (2) slow successes, and (3) failures. Our assumption is that slow successes and failures would not contribute to fast synaptic events. While failures not contributing is obvious, results from others (Erreger et al., 2005) as well as those in this manuscript using synaptic-like glutamate pulses confirm that slow successes arise solely from the long glutamate application (versus a brief synaptic-like pulse) and hence also would not contribute to fast signaling. Finally, while we are grouping slow successes and failures in the same category functionally, we do not know at present whether they share a kinetic or structural basis. Hence, our use of the term efficiency should not be confused with this term used in other contexts (Nayak et al., 2019; Indurthi and Auerbach, 2023).

Defining efficiency for individual patches

To define efficiency for individual patches, we initially identified a $t_{critical}$ based on the exponential fit to the cumulative

histogram, which was almost always two exponentials, using Jackson et al. (1983):

$$\frac{N_{fast}\exp^{-t_{crit}/\tau_{fast}}}{\tau_{fast}} = \frac{N_{slow}\exp^{-t_{crit}/\tau_{slow}}}{\tau_{slow}}$$

and specifically for $t_{critical}$:

$$-t_{critical} = \ln\left(\frac{\tau_{slow}}{\tau_{fast}}\frac{N_{fast}}{N_{slow}}\right) \cdot \frac{\tau_{slow}\tau_{fast}}{\tau_{fast} - \tau_{slow}}$$

For each patch, we would then use this $t_{critical}$ to define whether a success was in the fast ($<t_{critical}$) or slow ($>t_{critical}$) component, permitting calculation of an efficiency term for each individual patch. In instances where a single exponential was sufficient for the cumulative histogram, we assumed efficiency = successes.

Rationale for inclusion of patches in histograms and averages

For our cumulative histograms and averages, we included only patches that had at minimum 10 applications or trials. For rigor, we wanted to collect as many events as possible so that we could include all patches. However, there were many patches that were lost before 10 sweeps could be achieved. For arbitrary reasons, we decided that 10 trials were the minimum necessary to ensure that they were "representative" of the broader dataset (this also aided in defining single-channel patches). A larger number of events, perhaps 50, would certainly be more representative, but this would exclude many patches, thus limiting the sample size. A review of patches with 10 to 20 events indicates that they fall within the averages of patches with more events.

Statistics

Data analysis was performed using IgorPro (Wavemetrics), Excel (Microsoft), ChannelLab (Stephen Traynelis), and GraphPad (Prism). Results from the Igor analysis for each recording were organized in a Microsoft Excel sheet. All average values are presented as mean ± SEM. For statistical analysis, we used GraphPad. In instances where we were comparing two means, we used an unpaired two-tailed Student's *t* test to test for significant differences. Statistical significance was typically set at $P < 0.05$. In instances where we were interested in how constructs varied from each other, we used an ANOVA and followed with Tukey's test ($P < 0.05$).

Results

To assay the activation efficiency of NMDARs, we applied glutamate for 1 s to outside-out patches containing a single channel (e.g., Fig. 1, A and B) (Amin et al., 2021). In terms of outcomes, we were interested in two features (see Materials and methods): (1) whether there was a success (the channel opened) versus a failure (no channel opening), and (2) if a success, the time interval between the start of the glutamate application to the first channel opening, referred to as "latency to first opening" (Aldrich et al., 1983). Both success rate and latency to first opening have physiological significance since they reflect how efficiently a transient glutamate signal is translated into channel opening.

Internal energy components facilitate receptor activation

Previously, we used a KCl-based internal solution without added energy components and our standard external solution at pH 8.0 and with no divalent to maximize gating (Amin et al., 2021) (18 patches). Here, we expanded on this data set for GluN1-1a/GluN2A by adding in four new patches, which yielded results similar to those published previously: Success rate for prior set, 82 ± 2% (n = 18) (mean ± SEM, n = number single-channel patches) versus new set, 75 ± 5% (n = 4) ($P = 0.09$, t test); Mean latency to first opening for prior set, 48 ± 8 ms versus 43 ± 12 ms ($P = 0.40$, t test).

We combined the results from Amin et al. (2021) (18 patches) plus the four new patches, all of which were done for GluN1/GluN2A and using our energy-free internal. In this data set, we recorded from 22 different outside-out patches with the number of applications varying from 10 to 636 per patch. There was a total of 2,053 applications, of which 527 were failures (Table 1). Thus, the success rate of agonist binding inducing channel opening was 80 ± 2% (n = 22), whereas the global success rate was 74% (1,526 successful events out of 2,053 total applications). For successes, the mean latency to first opening was 47 ± 7 ms (Table 1). The latency dwell time histogram was best characterized by two exponentials: a fast (τ = 6.8 ms, 89.6%) and a slow (τ = 373.7 ms, 10.4%) component (Fig. 1 C), values indistinguishable from those in Amin et al. (2021).

To begin to address activation efficiency under different conditions, especially those more physiologically relevant, we initially tested an internal solution containing added ATP and GTP that we refer to as "energy-based" (see Materials and methods) (Fig. 1, A and B). The presence of energy-based internal significantly reduced the failure rate (success rate 93 ± 3%, n = 6) compared with the condition without such components (about 80%) (Fig. 1 E). Again, the latency dwell time histogram was best characterized by two exponentials (fast, τ = 6.7 ms, 96.2%; slow, τ = 423.2, 3.8%) (Fig. 1 D). While the time components were very comparable to those in the absence of energy components, the fractions were changed, being shifted to the fast component, from 90% to 96%.

To summarize the success rate and the latency to first open, we defined activation "efficiency" (η), which is the fraction of the fast component out of the total number of trials (η = total trials - failures – fraction of slow component) (see Materials and methods). We assume this efficiency term reflects the fraction of the total glutamate-releasing events that would contribute to fast synaptic signaling. Without energy internals, η was 0.72 ± 0.02, n = 22, suggesting that at most 72% of release events could lead to a synaptic event. In contrast, with the energy-based internal, efficiency was significantly enhanced to 0.90 ± 0.04, n = 6 (Fig. 1 F and Table 1).

Overall, these results suggested that the status of the intracellular C-terminal domain (or some other intracellular component), such as whether it is phosphorylated or not, influences activation efficiency, highlighting that this kinetic component is

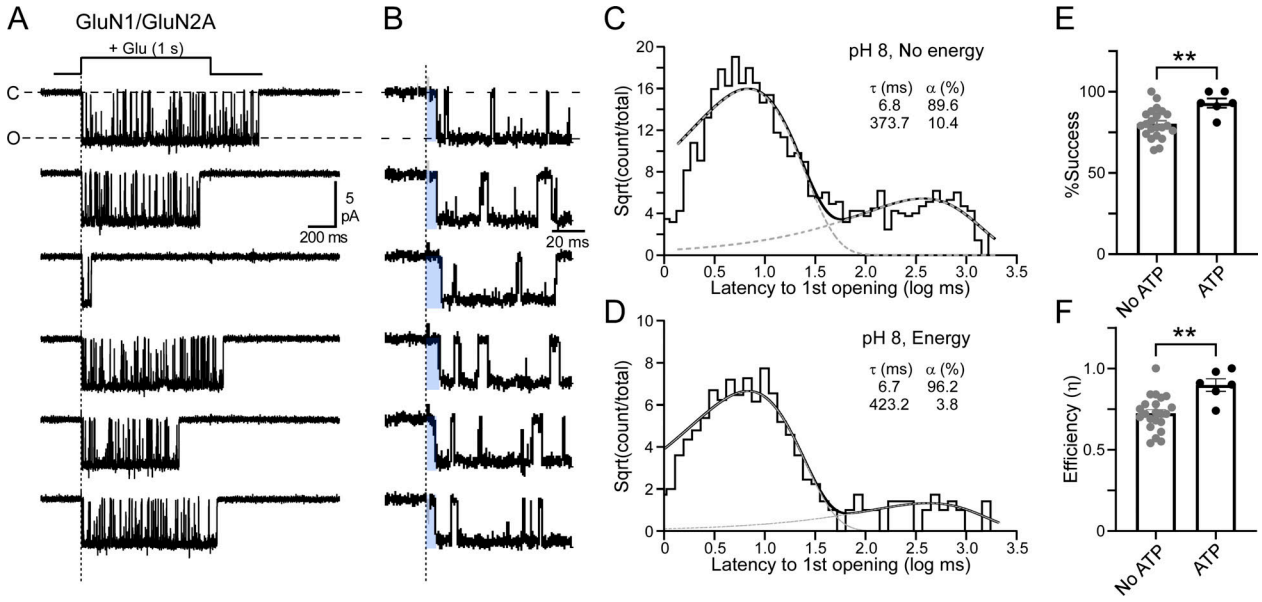

Figure 1. **An energy-based internal solution enhances activation efficiency. (A and B)** Membrane currents for a single wild-type GluN1-1a/GluN2A channel in an outside-out patch (six consecutive traces). Single channel openings are downward deflections (C, closed; O, open). Dashed vertical line indicates the start of a 1-s glutamate (1 mM) application in the continuous presence of glycine (0.1 mM). Traces in B are those in A but on an expanded time scale. Blue highlights illustrate variations to delays to first opening. Currents were sampled at 50 kHz (displayed at ~1 kHz). Holding potential, −60 mV. The external solution was our standard external solution at pH 8, and the pipette solution (energy-based) contained added ATP and GTP (see Materials and methods). **(C and D)** Dwell time histogram (Sqrt, Square root) of the latency to first opening, the time between the start of agonist application to the first channel opening. For both histograms, our standard external solution was at pH 8 with the internal solution containing either no added ATP or GTP (C), as in Amin et al. (2021) or added ATP and GTP (D) (raw currents illustrated in A and B). Both histograms were best fit by two exponentials (dashed lines). The no energy internal, external at pH 8 includes results from Amin et al. (2021) (18 patches) plus four additional patches. **(E)** Success rate (1 − failure rate) (mean ± SEM) for averages from patches with a minimum of 20 trials (circles represent individual data points). See Table 1 for additional details. **P < 0.01, Student's *t* test, P = 0.004. **(F)** Efficiency (η) of activation (mean ± SEM) for all patches. η is the fraction of the total number of trials that are present within the fast component of the latency histogram and represents the fraction of events that would contribute to fast synaptic transmission. **P < 0.01, Student's *t* test, P = 0.0014.

regulated. While extremely intriguing, we do not explore the basis for this enhancement further here.

Longer recovery times between applications enhance the efficiency of channel activation

Failures as well as the slow component may reflect that receptors are in a "desensitized" state after exposure to glutamate. The time course for recovery of at least GluN1/GluN2A receptors is around 0.9 s (Alsaloum et al., 2016). To assess the contribution of desen sitization to the failure observed, we extended the time between the start of glutamate applications from 4 to 10 s (since the application itself was 1 s in duration, the delay between the end to the start of the next application went from 3 to 9 s) (Fig. 2, A and B).

Table 1. **Summary of patches/events under different physiological conditions**

Construct	Internal soln	pH	Interval (s)	Total events (total # of patches)	Average latency (ms)	Successes % (global)	Efficiency (t_{crit})
rN1-1a/ rN2A	No ATP, GTP	8	4	2,053 (22)	47 ± 7	80 ± 2 (74)	0.72 ± 0.02 (42.7)
	ATP and GTP	8	4	559 (6)	25 ± 8	93 ± 3 (91)	0.90 ± 0.04 (50.5)
	No ATP, GTP	8	10	789 (14)	22 ± 7	88 ± 3 (90)	0.86 ± 0.04 (59.7)
	ATP and GTP	8	10	583 (12)	23 ± 6	93 ± 2 (91)	0.90 ± 0.02 (52.9)
	ATP and GTP	7.4	10	1,407 (21)	42 ± 7	83 ± 2 (85)	0.78 ± 0.02 (70.1)

Values shown are mean ± SEM for average latency of the delay to first opening, Successes (average of successes for individual patches), and Efficiency (= [successes − slow component]/total trial number); see Materials and methods). The number below the total events shows the total number of patches recorded (a patch required a minimum of 10 trials to be included). Global successes (total number successes/total number of trials) and t_{crit} are indicated in the last two columns. Recordings were made under different conditions: an internal solution either containing no ATP and GTP (energy-free) or one containing these elements (energy-based); our standard external solution at pH 8 or 7.4; and/or a delay between the start of glutamate applications of 4 or 10 s. All constructs are rats. Single channels were recorded in the outside-out mode at −60 mV (e.g., Fig. 1) and analyzed in Igor Pro (see Materials and methods).

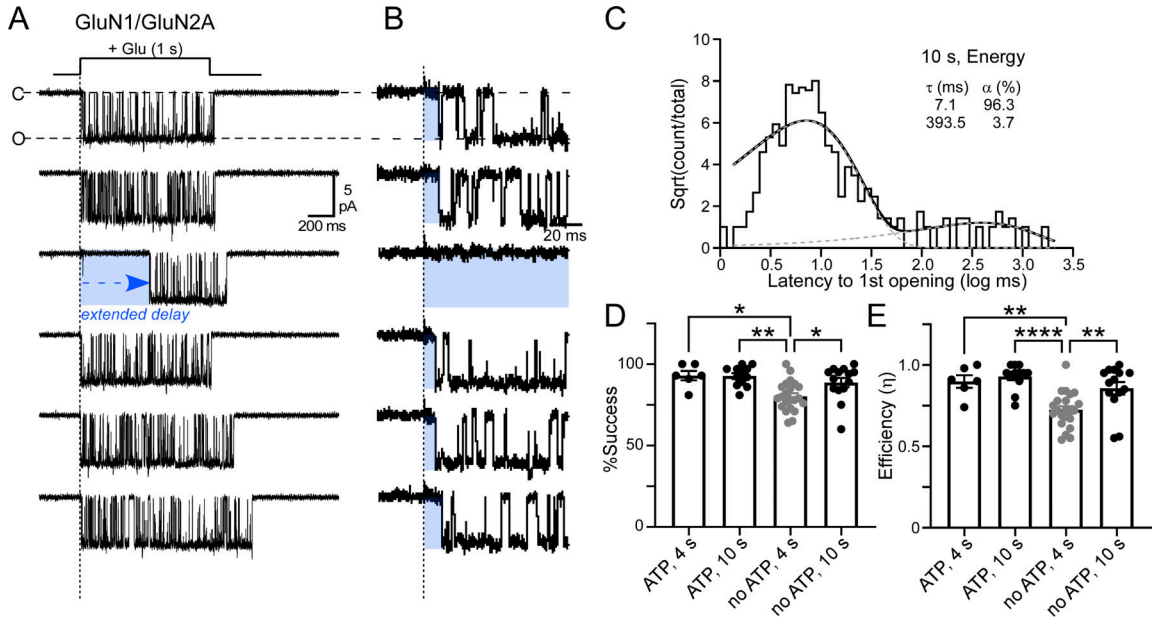

Figure 2. **Increasing the time for recovery between applications increases activation efficiency.** Single-channel openings with a delay of 10 s between the start of each consecutive application versus a delay of 4 s. **(A and B)** Currents with a 10-s delay in our standard external solution at pH 8 with an energy-based internal. Displayed as in Fig. 1. **(C)** Dwell time histogram of the latency to first opening with a 10-s delay and an energy-based internal. Histogram was best fit by two exponentials (dashed lines). **(D)** Mean (±SEM) success rate for various conditions. *P < 0.05, **P < 0.01, one-way ANOVA (P = 0.0005) with a post-hoc Tukey's test. No ATP, 4 s is statistically different from all other conditions: versus ATP, 4 s (P = 0.015), versus ATP, 10 s (P = 0.0013), versus no ATP, 10 s (P = 0.035). All other comparisons were not statistically different: ATP, 4 s versus ATP, 10 s (P > 0.99), ATP, 4 s versus no ATP, 10 s (P = 0.75), ATP, 10 s versus no ATP, 10 s (P = 0.65). **(E)** Mean (±SEM) efficiency (η) of activation for various conditions. **P < 0.01, ****P < 0.001, one-way ANOVA (P < 0.0001) with a post-hoc Tukey's test. No ATP, 4 s is statistically different from all other conditions: versus ATP, 4 s (P = 0.0074), versus ATP, 10 s (P < 0.0001), versus no ATP, 10 s (P = 0.0056). All other comparisons were not statistically different: ATP, 4 s versus ATP, 10 s (P = 0.95), ATP, 4 s versus no ATP, 10 s (P = 0.87), ATP, 10 s versus no ATP, 10 s (P = 0.38). Note that "not significant" comparisons are not indicated.

For 10-s recovery times and using our energy-based internal (ATP, 10 s), the dwell time histogram was best fit by two exponentials (Fig. 2 C) with parameters comparable with those at 4 s with the same internal (ATP, 4 s) (Fig. 2 D and Table 1). Hence, the 10–15% failures and slow components occurring under these conditions are presumably not due to some form of desensitization. However, we also recorded using our energy-free internal and contrasted latency between 4 (no ATP, 4 s) and 10 s (no ATP, 10 s) delays (Fig. 2 D and Table 1). The increase to a 10-s delay without energy internal significantly increased successes but again to a maximum level comparable with what was recorded with the energy-based internal. Indeed, in terms of efficiency, the 10-s recovery times, either with or without the energy internal, were indistinguishable (Fig. 2 E and Table 1). Hence, even under presumed optimized conditions, there remained about a 10–15% inefficiency.

Protons impede receptor activation efficiency

NMDARs are highly sensitive to protons (Traynelis and Cull-Candy, 1991; Dravid et al., 2007; Hansen et al., 2021). To test proton action on activation efficiency, we recorded using our standard external solution, but now at pH 7.4 (Fig. 3, A and B and Table 1). Notably, fits to the dwell-time histogram for the latency to first opening for GluN1/GluN2A NMDARs at pH 7.4 still required two kinetic components (Fig. 3 C). However, these components were shifted rightward relative to those in pH 8.0 with the fast component around 10–11 ms whereas it was around 7 ms at pH 8.0. In addition, these NMDARs activation at pH 7.4 showed significantly reduced successes (Fig. 3 D) and reduced efficiency (Fig. 3 E).

Hence, and comparable to previous studies for rodent subunits, where NMDARs are highly sensitive to changes in local protons, we found a reduction in gating, in this case activation efficiency, at physiological pH compared with pH 8.0. For all experiments moving forward, and unless noted otherwise, we use the internal (energy-based) and external (pH 7.4) solutions as in Fig. 3 with a 10-s delay between applications.

GluN2B-containing receptors show reduced activation efficiency

The two major GluN2 subunits in the nervous system are GluN2A and GluN2B (Sheng et al., 1994; Hansen et al., 2021). To begin to address the activation efficiency of GluN2B-containing receptors, we shifted from rodent to human constructs and assayed the activation efficiency of human GluN1/GluN2A and GluN1/GluN2B receptors (Fig. 4, A–C and Table 2). Notably, rodent and human GluN1/GluN2A receptors showed no significant difference between success rates, efficiency (Fig. 4 D), or average latency to first opening (Fig. 4 D).

For human GluN1/GluN2B receptors (Fig. 4, A and B), fits to the dwell-time histogram for the latency to first opening, like for GluN1/GluN2A, required two kinetic components (Fig. 4 C).

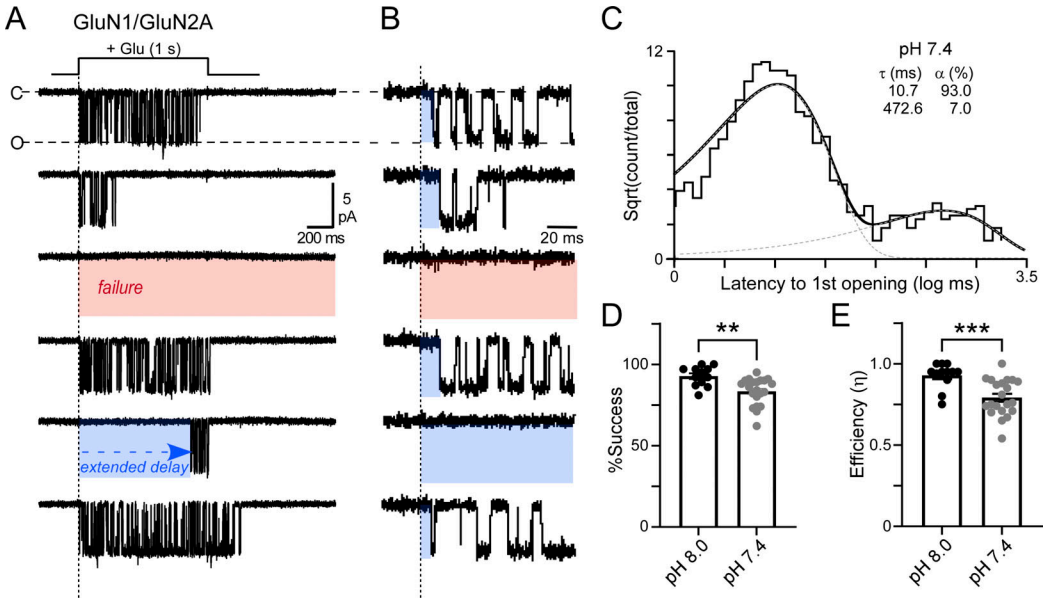

Figure 3. **Activation efficiency is reduced at physiological pH.** Single-channel openings at pH 7.4, all with an energy-based internal and a 10-s delay, as a comparison versus standard external solution at pH 8.0. **(A and B)** Currents at pH 7.4 with a 10-s delay between applications. **(C)** Dwell time histogram of the latency to first opening with a 10-s delay and an energy-based internal. The histogram was best fit by two exponentials (dashed lines). **(D)** Mean (±SEM) success rate. **P < 0.01, Student's *t* test, P = 0.002. **(E)** Mean (±SEM) efficiency (η) of activation. ***P < 0.001, Student's *t* test, P = 0.0008.

However, these components were shifted far rightward (slower) than for GluN1/GluN2A. For example, the fast component for GluN1/GluN2B was around 36 ms whereas for GluN2A-containing receptors it was around 10–11 ms. Further, for GluN2B-containing receptors, efficiency was significantly reduced (Fig. 4 D) and the average latency to activation was significantly slower (Fig. 4 E). Hence, and comparable with previous results for rodent subunits (Chen et al., 1999; Erreger et al., 2005; Tian et al., 2021), GluN2A-containing NMDARs show a more rapid and greater likelihood of channel activation. These results further highlight that there are fundamental differences in the activation mechanism between GluN2A- and GluN2B-containing receptors.

Brief synaptic-like agonist applications

For our experiments, we used 1-s glutamate applications because they facilitate identifying single-channel patches and allow more events to be collected, permitting more rigorous analysis of latency to first opening (see Materials and methods). To address activation of GluN2A- and GluN2B-containing receptors with more physiological glutamate exposures, we applied glutamate to single-channel patches using 2-ms glutamate applications (Fig. 5) (see Materials and methods for rationale of 2-ms pulses).

Brief (2-ms) glutamate applications to GluN1/GluN2A (Fig. 5 A) or GluN1/GluN2B (not shown) receptors resulted in failures as well as variations in the delay to first opening (Erreger et al., 2005). As for 1-s applications, the latency histogram for GluN1/GluN2A showed two components, with the fast component (5.6 ms) faster than that for 1-s application (about 10 ms) (Fig. 5 B). We were unable to perform a comparable histogram analysis for GluN2B-containing receptors because of fewer events and wider variations in the delays. For the 2-ms and 1-s application for GluN1/GluN2A, the rising phase of the histograms was comparable (Fig. 5 C). Hence, the faster activation component for 2-ms applications most likely reflects that the 1- application generates more "fast" events with a longer latency (shifting the histogram fit to the right) that do not occur with the 2-ms application (Fig. 5 C).

Overall, GluN1/GluN2A receptors showed fewer successes in the 2-ms application compared to the 1-s application (Table 3) as well as a reduced efficiency (Fig. 5 D, left) but no differences in the average latency (Fig. 5 D, right). GluN2B-containing receptors showed a similar pattern of activity in terms of success rates (Table 3) and average latency (Fig. 5 E, right). In contrast, the efficiency between 2 ms and 1 s for GluN2B-containing receptors was not different (Fig. 5 E, left). Hence, from a physiological perspective, the 1-s application for GluN2A-containing receptors overestimates the efficiency of activation whereas that for GluN2B-containing receptors does not. We assume this reflects the more rapid activation of GluN2A-containing receptors (see Discussion). Nevertheless, for technical reasons—identifying single-channel patches—we continue to use 1-s applications. In addition, in terms of receptor activation, both application times reveal the same mechanism of activation (Fig. 5 C) and a strong difference in the delay to activation between GluN2A- and GluN2B-containing receptors (Fig. 5, D and E).

Activation efficiency of putative triheteromeric GluN1/GluN2A/GluN2B receptors

In the brain, NMDARs exist both as diheteromeric (containing 2 GluN1 plus 2 GluN2A or 2 GluN2B subunits) and triheteromeric (containing two GluN1 plus 1 GluN2A and 1 GluN2B subunit) receptors (Rauner and Köhr, 2011; Tovar et al., 2013;

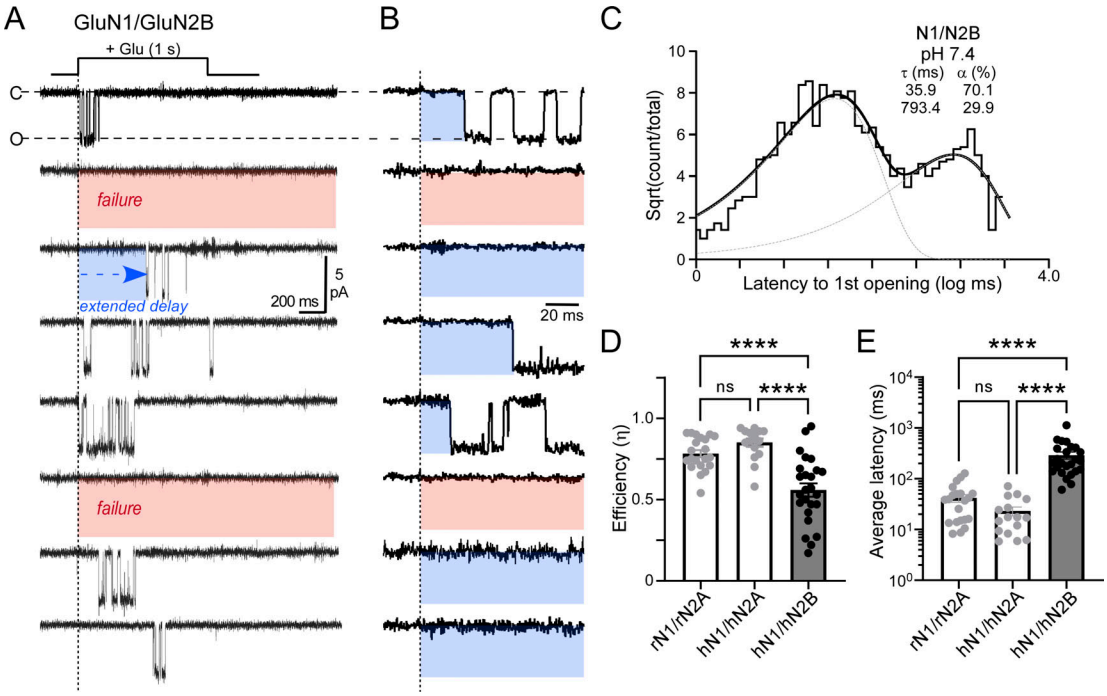

Figure 4. **GluN2B-containing receptors show a reduced activation efficiency. (A and B)** Currents from a patch containing a single human GluN1/GluN2B receptor. External solution is our standard at pH 7.4 with an energy-based internal (see Table 2). **(C)** Dwell time histogram of the latency to first opening for GluN1/GluN2B channels. The histogram was best fit by two exponentials (dashed lines). **(D)** Mean (±SEM) efficiency (η) of activation for various constructs, either rat (r) or human (h) N1/N2A (rN1/rN2A, hN1/hN2A) or human N1/N2B (hN1/hN2B). ****P < 0.0001, one-way ANOVA (P < 0.0001) with a post-hoc Tukey's test: rN2A versus hN2A, P = 0.37; rN2A versus hN2B, P < 0.0001; hN2A versus hN2B, P < 0.0001. **(E)** Average delay (mean ± SEM) for various constructs. Note log scale. ****P < 0.0001, one-way ANOVA (P < 0.0001) with a post-hoc Tukey's test: rN2A versus hN2A, P = 0.93; rN2A versus hN2B, P < 0.0001; hN2A versus hN2B, P < 0.0001.

Hansen et al., 2021). To assay putative GluN1/GluN2A/GluN2B receptors, we took advantage of an approach that constrains membrane expression to triheteromeric receptors (see Materials and methods) (Hansen et al., 2014) (Fig. 6). It should be noted that since these are single-channel recordings, we cannot rule out that there was leakage of diheteromeric GluN2A/GluN2A receptors, and so they must be viewed as "putative" triheteromeric receptors.

Control constructs for the triheteromeric system showed activation parameters indistinguishable from those of corresponding wild-type constructs (Table 4). Putative triheteromeric GluN1/GluN2A/GluN2B receptors showed robust activation (Fig. 6, A and B) with the histogram fit by a single exponential (Fig. 6 C). The fit to the histogram (τ = 8.3 ms) was comparable albeit somewhat faster than that for diheteromeric GluN1/GluN2A receptors (τ = 10–11 ms), and it was only a single exponential fit. Since control constructs were not significantly different from our wild-type human GluN2A- and GluN2B-containing constructs (Table 4), we compared the triheteromeric results to these constructs (Fig. 6, D and E). Efficiency and average delay were not significant between the triheteromeric construct and GluN1/GluN2A whereas GluN1/GluN2B showed a reduced efficiency and a slower average activation. Hence, overall the triheteromeric receptors display an activation efficiency comparable with, if not more efficient, than GluN2A diheteromeric receptors. These findings align with the general

Table 2. **Summary of patches/events for different human NMDAR subunits**

Construct	Internal soln	pH	Interval (s)	Total events (# of patches)	Average latency (ms)	Successes % (global)	Efficiency (t_{crit})
rN1/rN2A	ATP	7.4	10	1,407 (21)	42 ± 7	83 ± 2 (85)	0.78 ± 0.02 (69.8)
hN1/hN2A	"	"	"	469 (16)	23 ± 5	87 ± 2 (88)	0.85 ± 0.03 (70.1)
hN1/hN2B	"	"	20	1,234 (25)	290 ± 50	76 ± 3 (76)	0.56 ± 0.04 (148)
hN1/hN2C	"	"	10	660 (18)	76 ± 9	97 ± 1 (97)	0.92 ± 0.02 (284)
hN1/hN2D	"	"	"	486 (10)	74 ± 15	98 ± 1 (98)	0.92 ± 0.02 (201)

Values are displayed as in Table 1. For all recordings, our internal solution was energy-based (ATP and GTP), the external solution was our standard external solution at pH 7.4; and there was a 10- or 20-s delay between applications. Constructs are either rat (r) or human (h). In all instances, the GluN1 subunit was the GluN1-1a splice variant.

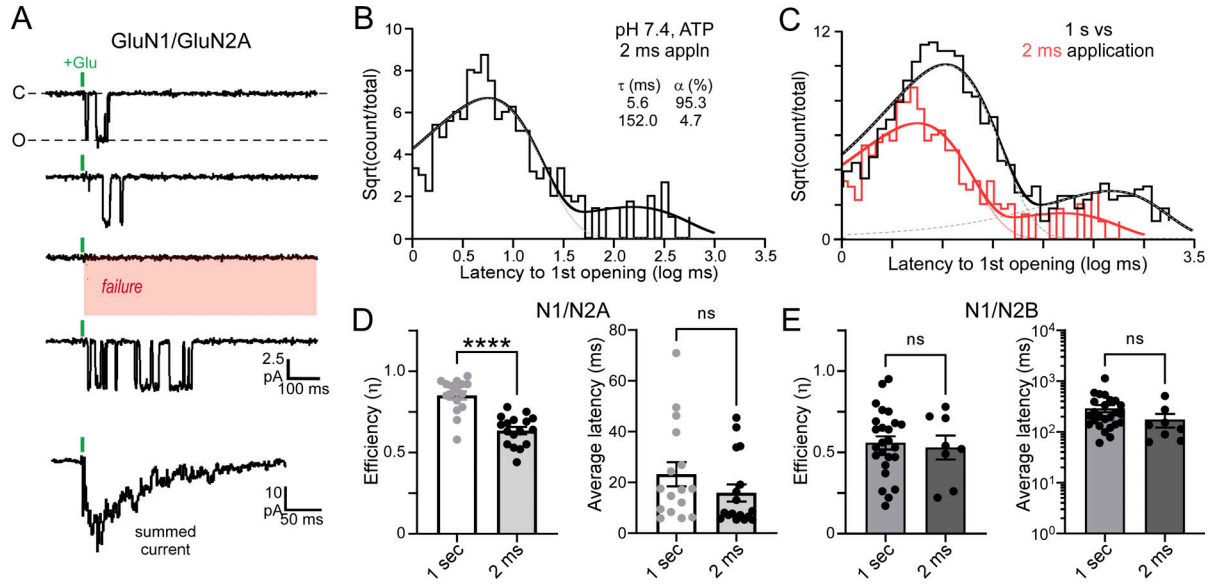

Figure 5. **Activation of human GluN2A and GluN2B receptors in response to brief synaptic-like (2-ms) glutamate applications. (A)** Currents from a patch containing a single human GluN1/GluN2A receptor in response to a 2-ms glutamate application (see Table 3). External solution is our standard at pH 7.4 with an energy-based internal (see Materials and methods). The bottom trace is the summed response to multiple (50 total) glutamate applications. **(B)** Dwell time histogram of the latency to first opening. The histogram was best fit by two exponentials (dashed lines). **(C)** Overlay of dwell time histograms of the latency to first opening for 1-s or 2-ms (red) applications. **(D and E)** Mean (±SEM) efficiency (η) of activation (left) and average latency (right) for GluN2A- (D) or GluN2B- (E) containing receptors. ****P < 0.0001, Student's *t* test: GluN2A efficiency, P < 0.0001, latency, P = 0.21; GluN2B efficiency, P = 0.73, latency, P = 0.19. Note for synaptic-like glutamate applications, the success rate and efficiency are the same.

observation that triheteromeric GluN1/GluN2A/GluN2B receptors often display gating activity comparable with diheteromeric GluN1/GluN2A receptors (Hansen et al., 2014; Sun et al., 2017).

Activation efficiency of GluN2C- and GluN2D-containing receptors

GluN2C- and GluN2D-containing NMDARs display distinct single channel activity compared with GluN2A-containing receptors (Dravid et al., 2008; Traynelis et al., 2010; Vance et al., 2013). To assay the activation efficiency of GluN2C- and GluN2D-containing receptors, we applied 1-s glutamate applications to patches containing presumed single GluN1/GluN2C receptor (Fig. 7, A and B) or GluN2D- (Fig. 7, C and D) containing receptors. The challenge with these experiments is that GluN2C- and GluN2D-containing receptors display low Popen including brief mean-open-times, making detection of single-channel patches difficult (see Materials and methods). Numerous patches were rejected because of the clear presence of multiple channels. Nevertheless, for some patches, we cannot rule out that they contain multiple channels.

The latency dwell time histograms for GluN2C- and GluN2D-containing receptors were best characterized by two exponentials: for GluN2C, a fast (τ = 68 ms, 85%) and a slow (τ = 302 ms, 15%) component (Fig. 7 E); whereas for GluN2D, a fast (τ = 42 ms, 89%) and a slow (τ = 311 ms, 11%) component (Fig. 7 F).

Comparing diheteromeric constructs, GluN2C- and GluN2D-containing receptors showed success rates somewhat greater than those for GluN1/GluN2A, whereas all these subunits showed a significantly higher success rate than GluN1/GluN2B (Fig. 8 A and Table 2). On the other hand, efficiency was not significantly different between GluN2A-, GluN2C-, and GluN2D-containing receptors but was significantly reduced in GluN2B-containing receptors (Fig. 8 B). Finally, the average latency was

Table 3. **Summary of patches/events for brief application**

Construct	Internal soln	pH	Interval (s)	Total events (# of patches)	Average latency (ms)	Successes % (global)	Efficiency (t_{crit})
hN1/hN2A (1 s)	ATP	7.4	10	469 (16)	23 ± 5	87 ± 2 (88)	0.85 ± 0.03 (70.1)
hN1/hN2A (2 ms)	"	"	"	710 (17)	16 ± 3	64 ± 2 (64)	0.64 ± 0.02 nc
hN1/hN2B (1 s)	"	"	20	1,234 (25)	290 ± 50	76 ± 3 (76)	0.56 ± 0.04 (148)
hN1/hN2B (2 ms)	"	"	"	426 (8)	180 ± 50	53 ± 7 (51)	0.53 ± 0.07 nc

Values are displayed as in Table 1. Glutamate applications were either 1 s or 2 ms in duration. All constructs are human. Note for synaptic-like pulses, the success rate and efficiency are the same, so a $t_{critical}$ was not calculated (nc).

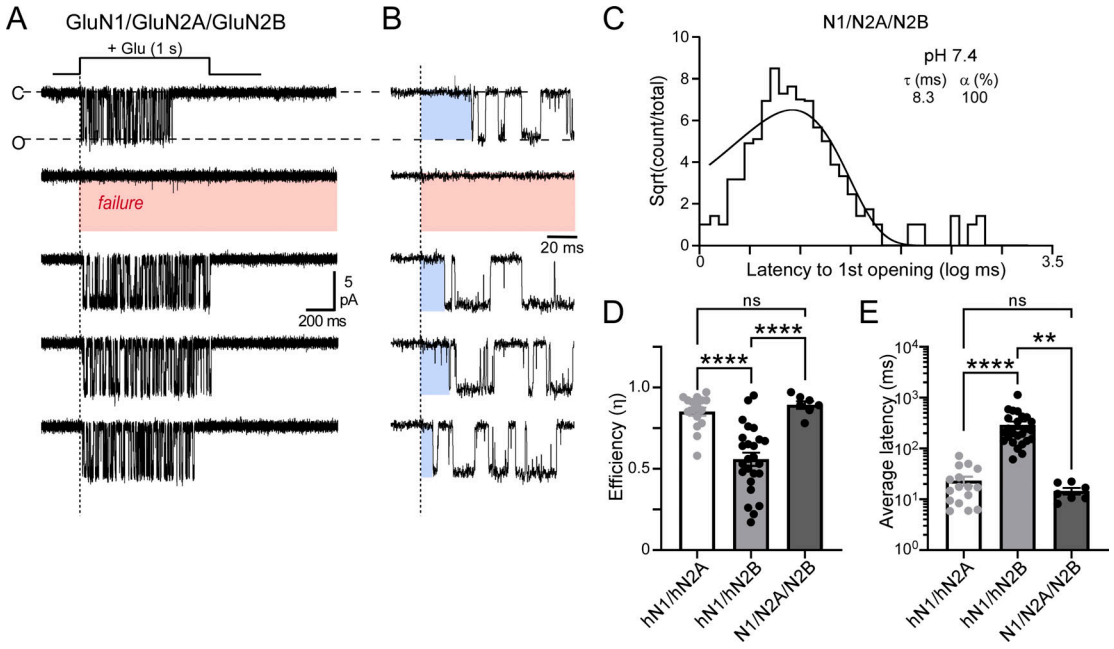

Figure 6. **Activation of presumed triheteromeric GluN2A and GluN2B receptors. (A and B)** Currents from a patch containing a single presumed GluN1/GluN2A/GluN2B receptor in response to 1-s glutamate applications. See Table 4 for additional details. **(C)** Dwell time histogram of the latency to first opening for presumed triheteromeric receptors. The histogram was best fit by a single exponential (solid line). **(D and E)** Mean (±SEM) efficiency (η) of activation (D) or average latency (E) for diheteromeric GluN1/GluN2A or GluN1/GluN2B receptors or triheteromeric GluN1/GluN2A/GluN2B receptors. **(D)** ****P < 0.0001, one-way ANOVA (P < 0.0001) with a post-hoc Tukey's test: N2A versus N2B, P < 0.0001; N2A versus N2A/N2B, P = 0.84, N2B versus N2A/N2B, P < 0.0001. **(E)** ****P < 0.0001, one-way ANOVA (P < 0.0001) with a post-hoc Tukey's test: N2A versus N2B, P < 0.0001; N2A versus N2A/N2B, P = 0.99, N2B versus N2A/N2B, P < 0.0012. h, human.

indistinguishable across GluN2A-, GluN2C-, and GluN2D-containing receptors but significantly faster than those receptors containing GluN2B (Fig. 8 C).

In summary, with 1-s applications (these patterns might be different with brief synaptic like applications), the activation mechanism for GluN2A-, GluN2C-, and GluN2D- is more comparable than for GluN2B-containing receptors.

Discussion

Here, we assayed the activation efficiency of rodent GluN1/GluN2A (and GluN1/GluN2B in the triheteromeric system) and human GluN2A-, GluN2B-, GluN2C-, and GluN2D-containing NMDARs by measuring success rates and the latency to first opening for outside-out single-channel patches. Previously, to maximize activation of GluN1/GluN2A receptors, we used conditions to prevent divalent (no Ca^{2+}, EDTA) and proton (pH 8.0) inhibition (Amin et al., 2021). Notably, under such conditions and using a 4-s delay between the start of glutamate applications, we observed a high number of failures (about 20%) and a low activation efficiency (0.72). We find that certain manipulations, including using an energy-based internal solution (Fig. 1) and increasing the time between applications (Fig. 2), increased efficiency, but even under optimized conditions and with a 1 s application, there was still about a 10–15% inefficiency for GluN1/GluN2A, which was further reduced at physiological

Table 4. **Summary of patches/events for triheteromeric system**

Construct	Internal soln	pH	Interval (s)	Total events (# of patches)	Average latency (ms)	Successes % (global)	Efficiency (t_{crit})
hN1/hN2A (Table 2)	ATP	7.4	10	469 (16)	23 ± 5	87 ± 2 (88)	0.85 ± 0.03 (70.1)
rN1/rN2A C1/C2	no ATP	7.4	10	506 (8)	31 ± 13^{ns}	87 ± 4^{ns} (89)	nc
hN1/hN2B (Table 2)	ATP	7.4	20	1,234 (25)	290 ± 50	76 ± 3 (76)	0.56 ± 0.04 (148)
rN1/rN2B C1/C2	no ATP	7.4	20	360 (8)	190 ± 55^{ns}	84 ± 4^{ns} (81)	nc
rN1 rN2A/rN2B	no ATP	7.4	10	509 (7)	14.5 ± 2	89 ± 2 (92)	0.89 ± 0.02[a]

Values are displayed as in Table 1. Glutamate applications were 1 s in duration. Parameters for the C1/C2 constructs were not significantly different (ns) from their respective wild-type constructs (Student's *t* tests): hN2A versus N2A C1/C2 successes, P = 0.94, average latency, P = 0.53; hN2B versus N2B C1/C2 successes, P = 0.13, average delay, P = 0.26. nc, not calculated. h, human; r, rat.
[a]Only a single exponential was needed for fit so success rate = efficiency.

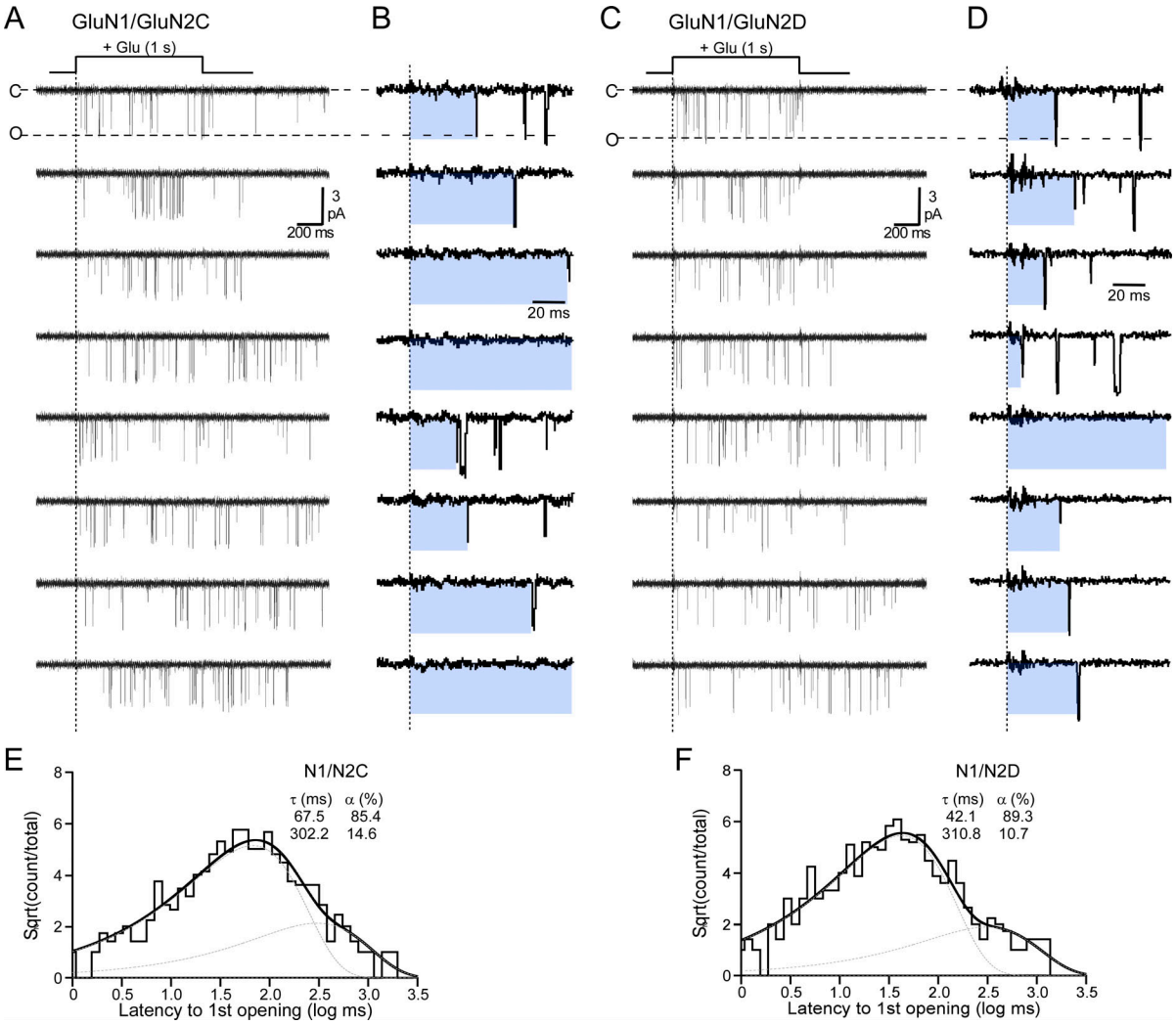

Figure 7. **Activation of human GluN2C and GluN2D receptors. (A–D)** Currents from patches containing a presumed single human GluN1/GluN2C (A and B) or a GluN1/GluN2D (C and D) receptor in response to 1-s glutamate applications. See Table 2 for additional details. **(E and F)** Dwell time histogram of the latency to first opening for GluN1/GluN2C (E) or GluN1/GluN2D (F) receptors. Both histograms were best fit by two exponentials (dashed lines).

pH (Fig. 3). Of the different GluN2 subunits, GluN2B-containing NMDARs showed the most dramatic failure rate and delays to opening (Fig. 4 and Fig. 8), highlighting that GluN2B subunit has the most distinct activation mechanism. The mechanistic and structural basis for the activation mechanism of the various GluN2 subunits remains unknown.

Most of our experiments were done with a 1-s pulse, as this aided in data collection (see Materials and methods). However, we also made synaptic-like glutamate pulses (2 ms, see Materials and methods) for GluN1/GluN2A and GluN1/GluN2B (Fig. 5). With synaptic-like applications, the success rate defines efficiency. Notably, the success rate for GluN1/GluN2A was 64%, less than the efficiency measured with 1-s pulses (0.85) (Table 3). For GluN1/GluN2B, the success rate measured with 2-ms pulses was 53%, same as that measured with 1-s pulses (0.56). For the fast-activating GluN1/GluN2A, we assume that the difference in efficiency between 2 ms and 1 s reflects that the 1-s pulse captures additional slower activation events in the fast component of the histogram (Fig. 5 C; note the rising phase is comparable but the peak is shifted rightward for 1 s). Despite this difference, the 2-ms pulses generally validate our definition of efficiency for 1-s pulses (see Materials and methods) with the caveat for GluN1/GluN2A, and the 1-s pulses overestimate efficiency. Nevertheless, to rigorously test the synaptic dynamics of GluN1/GluN2A receptors requires brief synaptic-like glutamate pulses.

Energy-based internal enhances receptors activation efficiency

In our experiments, we transitioned from an internal solution lacking energy (no ATP or GTP) to one containing sources of free energy (ATP and GTP, see Materials and methods). This energy-based internal by itself significantly enhanced activation efficiency (Fig. 1). The specific basis for this outcome is not known, but most likely reflects that the status of the intracellular C-terminal domain (CTD) is altered in the presence of the energy components and changes in some way the structural elements involved in receptor gating (Rosenmund and Westbrook, 1993;

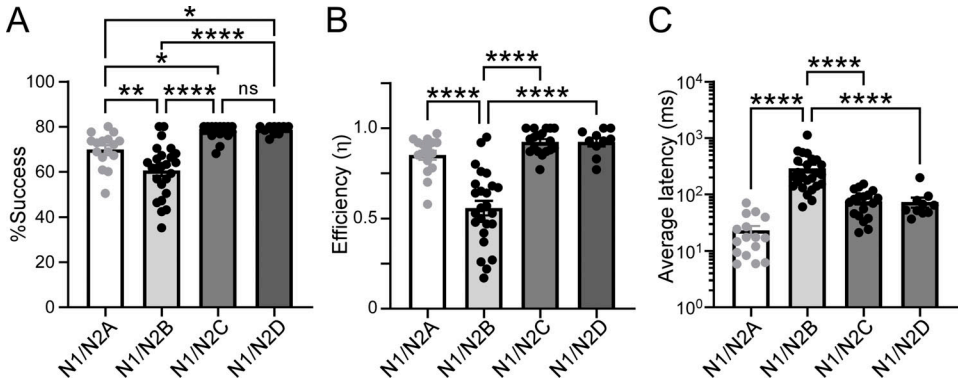

Figure 8. **Comparison of activation efficiency of different human NMDARs. (A)** Mean (±SEM) success rate: *P < 0.05, **P < 0.01, ****P < 0.0001, one-way ANOVA (P < 0.0001) with a post-hoc Tukey's test: N2A versus N2B, P = 0.0036, N2A versus N2C, P = 0.03, N2A versus N2D, P = 0.045; N2B versus N2C, P < 0.0001, N2B versus N2D, P < 0.0001; N2C versus N2D, P = 0.99. **(B)** Mean (±SEM) efficiency (η) of activation: ****P < 0.0001, one-way ANOVA (P < 0.0001) with a post-hoc Tukey's test: N2A versus N2B, P < 0.0001, N2A versus N2C, P = 0.44, N2A versus N2D, P = 0.58; N2B versus N2C, P < 0.0001, N2B versus N2D, P < 0.0001; N2C versus N2D, P > 0.99. **(C)** Mean (±SEM) average latency: ****P < 0.0001, one-way ANOVA (P < 0.0001) with a post-hoc Tukey's test: N2A versus N2B, P < 0.0001, N2A versus N2C, P = 0.70, N2A versus N2D, P = 0.81; N2B versus N2C, P < 0.0001, N2B versus N2D, P = 0.0008; N2C versus N2D, P > 0.99. See Table 2 for additional details. Note that "not significant" comparisons are not indicated.

Wang et al., 1993, 1996; Krupp et al., 2002; Bhatia et al., 2020). Indeed, a variety of posttranslational modifications of the CTD regulate receptor activation and gating (Salter et al., 2009; Murphy et al., 2014; Hansen et al., 2021; Mony and Paoletti, 2023).

How modulation of presumed intracellular sites enhances receptor activation is unclear. Some possible mechanisms include altered conformation of the CTD, which can impact receptor function (Choi et al., 2013) and may do so via the M4 segment (Amin et al., 2018; Hubalkova et al., 2021), and/or interactions with the lipid bilayer that change the lipid composition/organization proximal to the transmembrane domain (Korinek et al., 2015). Future experiments will be needed to further define this issue.

Different human GluN2 subunits

While we could assay rise times using summed currents for GluN2A-containing constructs (e.g., Amin et al., 2021), we were unable to do so consistently for GluN2B, GluN2C, or GluN2D constructs given the variability in latency to first opening. Nevertheless, the general pattern of activation (latency to first opening), GluN2A ~ GluN2C ~ GluN2D > GluN2B, parallels the rise times for rodent constructs: GluN2A about 5 ms (Amin et al., 2021) and 7 ms (Erreger et al., 2005); GluN2C about 4 ms (Dravid et al., 2008); GluN2D about 4.5 ms (Vance et al., 2012), and GluN2B about 12 ms (Erreger et al., 2005).

The diheteromeric GluN1/GluN2B receptors are the most inefficient subunit combination, having by far the fewest successes and the longest latency to first opening (Fig. 4 and Fig. 8). This highlights that the activation mechanism of GluN2B has major biophysical and structural differences from GluN2A subunits (Tian et al., 2021; Vyklicky et al., 2021). Open-state structures are now available for GluN1/GluN2B (Chou et al., 2024). Presumably, when GluN1/GluN2A open-state structures are available, there will be some difference in detail between these structures. On the other hand, GluN2C- and GluN2D-containing NMDARs displayed an activation efficiency not that dissimilar to GluN2A-containing (note GluN2C- and GluN2D-containing receptors tended to activate more slowly, but these differences were not significantly different). The major difference between GluN2C- and GluN2D-containing subunits is their much shorter mean open times (Traynelis et al., 2010). Hence, the process for the transition from agonist binding to channel opening may share characteristics between GluN2A-, GluN2C-, and GluN2D-containing receptors. New structures, as well as associated functional, optical, and molecular dynamic simulations, can help clarify the similarities and differences between the various subunits (Tian et al., 2021; Wang et al., 2021; Chou et al., 2022, 2024; Zhang et al., 2023; Bleier et al., 2024).

Mechanism of efficiency in NMDAR gating

Glutamate application to single-channel patches in NMDARs results in either successes (single-channel currents) or failures (no current). Similarly, the slow component of successes, which would not contribute to fast synaptic transmission as highlighted by brief applications (Fig. 5), further adds to the inefficiency of NMDAR activation. Failures and the slow components have physiological importance since a receptor would not contribute to synaptic current by the transmitter release event, and hence defining the mechanism is important to defining basic features of synaptic transmission.

In terms of NMDARs or ligand-gated ion channels in general, failures can arise from three general mechanisms: (1) Perhaps the most defined pathway, at least kinetically, is that the receptor has not recovered from a desensitized state induced by the previous glutamate exposure (Vance et al., 2013; Yao et al., 2013; Alsaloum et al., 2016). As would be expected, under our experimental conditions, increasing the recovery time between patches from 4 to 10 s potentiated gating efficiency. It is possible that the receptor still exists in a desensitized conformation after the 9-s delay though we think this is unlikely given that the tau of recovery is <1 s for GluN1/GluN2A (Alsaloum et al., 2016). (2)

Alternatively, failures may arise from inefficient events at the ligand-binding domain either because the agonist cannot bind or the agonist takes on the incorrect conformation in the binding pocket (Dolino et al., 2016; Yu and Lau, 2018; Yovanno et al., 2022). (3) The agonist may bind and activate the ligand-binding domain (i.e., close the clamshell), but the structural mechanisms coupling this conformational change, mainly in the linkers connecting the ligand-binding domain to the transmembrane domain (LBD-TMD linkers) (Talukder et al., 2010; Kazi et al., 2013, 2014; Ogden et al., 2017; McDaniel et al., 2020), to channel opening cannot overcome a local energy barrier. However, since no experimental condition eliminated failures, further research is necessary to fully understand the basis of failures in ion channel gating.

Synaptic implications of NMDAR activation efficiency

Our experiments did not address the impact of Ca^{2+} and Mg^{2+}, two critical physiological factors, on receptor activation. In addition, it is not clear that NMDARs are saturated with a single release event (Mainen et al., 1999), and we did not address the impact of sub-saturating glutamate (or glycine) concentrations on receptor activation. Nevertheless, our experiments reinforce the general principles of GluN2 subunit–specific gating and its regulation (Hansen et al., 2021; Mony and Paoletti, 2023), specifically, that GluN2A-containing receptors, either diheteromeric or triheteromeric, would be the fastest acting and efficient (Erreger et al., 2005; Hansen et al., 2014).

Previous work has highlighted that the kinetics of NMDAR activation plays a significant role in events at synapses (Lester et al., 1990; Rosenmund et al., 1995; Popescu et al., 2004). Our experiments with 2-ms glutamate pulses extend these findings and suggest interesting features of subunit-specific differences that are also supported by our 1-s pulses: GluN2A-containing receptors, either diheteromeric or triheteromeric, are activated more efficiency and with a reduced delay in comparison to GluN2B-containing diheteromeric receptors (Fig. 4, Fig. 5, and Fig. 6). In contrast, diheteromeric GluN2B-containing receptors while more inefficient also show a slower time course and a greater inconsistency of when activated (note the broader distribution of the fast component of the latency to first opening for GluN2A-(Fig. 3) versus GluN2B- (Fig. 4) containing receptors), suggesting that they would be less synchronized with a release event. Presumably, the more synchronized GluN2A-containing NMDARs would impact the dynamics of relief from Mg^{2+} block and Ca^{2+} influx in ways different from the less synchronized diheteromeric GluN2B-containing NMDARs. Nevertheless, these issues would have to be addressed specifically at synapses.

Conclusion

Assaying the latency to the first opening is a robust technique to elucidate the intricacy of ion channel gating dynamics and bridge the gap between agonist binding and channel activation. Clearly, the limitation of this approach is that it does not monitor events following the initial activation step, such as mean open time. Further, ultimately to fully resolve mechanisms of NMDAR activation will require a substantial number of events, far beyond those in the present study. To overcome experimental limitations and accurately reproduce the native features of synaptic NMDARs, careful selection of experimental conditions and a significantly large number of samples will be necessary.

Data availability

The datasets generated and analyzed during the current study are available from the corresponding authors upon reasonable request. The code used for analysis is available on GitHub (https://github.com/lwollmuth/HEKCell_Analysis).

Acknowledgments

Christopher J. Lingle served as the editor.

We thank Donna Schmidt for technical assistance and Drs. Amin and Kysilov for helpful discussions and/or comments on the manuscript as well as an anonymous reviewer for the suggested analysis of efficiency for individual patches. We also thank Dr. Stephen Traynelis and the Center for Functional Evaluation of Rare Variants for generously supplying human NMDAR constructs. We also thank Dr. Kasper Hansen for generously supplying us with the constructs for the triheteromeric system.

This work was supported by National Institutes of Health grant R01 NS088479 (L.P. Wollmuth) and Stony Brook University–Brookhaven National Laboratory seed grant (L.P. Wollmuth).

Author contributions: M. He: Conceptualization, Data curation, Formal analysis, Investigation, Methodology, Project administration, Resources, Software, Validation, Visualization, Writing - original draft, Writing - review & editing, L.P. Wollmuth: Conceptualization, Data curation, Formal analysis, Funding acquisition, Investigation, Methodology, Project administration, Resources, Software, Supervision, Validation, Visualization, Writing - original draft, Writing - review & editing.

Disclosures: The authors declare no competing interests exist.

Submitted: 9 July 2024
Revised: 28 September 2024
Revised: 2 November 2024
Accepted: 7 November 2024

References

Aldrich, R.W., D.P. Corey, and C.F. Stevens. 1983. A reinterpretation of mammalian sodium channel gating based on single channel recording. *Nature*. 306:436–441. https://doi.org/10.1038/306436a0

Alsaloum, M., R. Kazi, Q. Gan, J. Amin, and L.P. Wollmuth. 2016. A molecular determinant of subtype-specific desensitization in ionotropic glutamate receptors. *J. Neurosci.* 36:2617–2622. https://doi.org/10.1523/JNEUROSCI.2667-15.2016

Amin, J.B., A. Gochman, M. He, N. Certain, and L.P. Wollmuth. 2021. NMDA receptors require multiple pre-opening gating steps for efficient synaptic activity. *Neuron*. 109:488–501.e4. https://doi.org/10.1016/j.neuron.2020.11.009

Amin, J.B., X. Leng, A. Gochman, H.X. Zhou, and L.P. Wollmuth. 2018. A conserved glycine harboring disease-associated mutations permits NMDA receptor slow deactivation and high Ca^{2+} permeability. *Nat. Commun.* 9:3748. https://doi.org/10.1038/s41467-018-06145-w

Amin, J.B., C.L. Salussolia, K. Chan, M.C. Regan, J. Dai, H.X. Zhou, H. Furukawa, M.E. Bowen, and L.P. Wollmuth. 2017. Divergent roles of a

peripheral transmembrane segment in AMPA and NMDA receptors. *J. Gen. Physiol.* 149:661–680. https://doi.org/10.1085/jgp.201711762
Banke, T.G., and S.F. Traynelis. 2003. Activation of NR1/NR2B NMDA receptors. *Nat. Neurosci.* 6:144–152. https://doi.org/10.1038/nn1000
Bhatia, N.K., E. Carrillo, R.J. Durham, V. Berka, and V. Jayaraman. 2020. Allosteric changes in the NMDA receptor associated with calcium-dependent inactivation. *Biophys. J.* 119:2349–2359. https://doi.org/10.1016/j.bpj.2020.08.045
Bhattacharya, S., A. Khatri, S.A. Swanger, J.O. DiRaddo, F. Yi, K.B. Hansen, H. Yuan, and S.F. Traynelis. 2018. Triheteromeric GluN1/GluN2A/GluN2C NMDARs with unique single-channel properties are the dominant receptor population in cerebellar granule cells. *Neuron*. 99:315–328.e5. https://doi.org/10.1016/j.neuron.2018.06.010
Bleier, J., P.R. Furtado de Mendonca, C.H. Habrian, C. Stanley, V. Vyklicky, and E.Y. Isacoff. 2024. Subtype-specific conformational landscape of NMDA receptor gating. *Cell Rep.* 43:114634. https://doi.org/10.1016/j.celrep.2024.114634
Chen, N., T. Luo, and L.A. Raymond. 1999. Subtype-dependence of NMDA receptor channel open probability. *J. Neurosci.* 19:6844–6854. https://doi.org/10.1523/JNEUROSCI.19-16-06844.1999
Choi, D.W. 2020. Excitotoxicity: Still hammering the ischemic brain in 2020. *Front. Neurosci.* 14:579953. https://doi.org/10.3389/fnins.2020.579953
Choi, U.B., R. Kazi, N. Stenzoski, L.P. Wollmuth, V.N. Uversky, and M.E. Bowen. 2013. Modulating the intrinsic disorder in the cytoplasmic domain alters the biological activity of the N-methyl-D-aspartate-sensitive glutamate receptor. *J. Biol. Chem.* 288:22506–22515. https://doi.org/10.1074/jbc.M113.477810
Chou, T.H., M. Epstein, R.G. Fritzemeier, N.S. Akins, S. Paladugu, E.Z. Ullman, D.C. Liotta, S.F. Traynelis, and H. Furukawa. 2024. Molecular mechanism of ligand gating and opening of NMDA receptor. *Nature*. 632:209–217. https://doi.org/10.1038/s41586-024-07742-0
Chou, T.H., H. Kang, N. Simorowski, S.F. Traynelis, and H. Furukawa. 2022. Structural insights into assembly and function of GluN1-2C, GluN1-2A-2C, and GluN1-2D NMDARs. *Mol. Cell*. 82:4548–4563.e4. https://doi.org/10.1016/j.molcel.2022.10.008
Clements, J.D., R.A. Lester, G. Tong, C.E. Jahr, and G.L. Westbrook. 1992. The time course of glutamate in the synaptic cleft. *Science*. 258:1498–1501. https://doi.org/10.1126/science.1359647
Coyle, J.T. 2017. Schizophrenia: Basic and clinical. *Adv. Neurobiol.* 15:255–280. https://doi.org/10.1007/978-3-319-57193-5_9
Dolino, D.M., S. Rezaei Adariani, S.A. Shaikh, V. Jayaraman, and H. Sanabria. 2016. Conformational selection and submillisecond dynamics of the ligand-binding domain of the N-Methyl-d-aspartate receptor. *J. Biol. Chem.* 291:16175–16185. https://doi.org/10.1074/jbc.M116.721274
Dravid, S.M., K. Erreger, H. Yuan, K. Nicholson, P. Le, P. Lyuboslavsky, A. Almonte, E. Murray, C. Mosely, J. Barber, et al. 2007. Subunit-specific mechanisms and proton sensitivity of NMDA receptor channel block. *J. Physiol.* 581:107–128. https://doi.org/10.1113/jphysiol.2006.124958
Dravid, S.M., A. Prakash, and S.F. Traynelis. 2008. Activation of recombinant NR1/NR2C NMDA receptors. *J. Physiol.* 586:4425–4439. https://doi.org/10.1113/jphysiol.2008.158634
Erreger, K., S.M. Dravid, T.G. Banke, D.J. Wyllie, and S.F. Traynelis. 2005. Subunit-specific gating controls rat NR1/NR2A and NR1/NR2B NMDA channel kinetics and synaptic signalling profiles. *J. Physiol.* 563:345–358. https://doi.org/10.1113/jphysiol.2004.080028
Ferrer, C., H. Hsieh, and L.P. Wollmuth. 2018. Input-specific maturation of NMDAR-mediated transmission onto parvalbumin-expressing interneurons in layers 2/3 of the visual cortex. *J. Neurophysiol.* 120:3063–3076. https://doi.org/10.1152/jn.00495.2018
Glasgow, N.G., B. Siegler Retchless, and J.W. Johnson. 2015. Molecular bases of NMDA receptor subtype-dependent properties. *J. Physiol.* 593:83–95. https://doi.org/10.1113/jphysiol.2014.273763
Goldschen-Ohm, M.P., D.L. Capes, K.M. Oelstrom, and B. Chanda. 2013. Multiple pore conformations driven by asynchronous movements of voltage sensors in a eukaryotic sodium channel. *Nat. Commun.* 4:1350. https://doi.org/10.1038/ncomms2356
Hansen, K.B., K.K. Ogden, H. Yuan, and S.F. Traynelis. 2014. Distinct functional and pharmacological properties of Triheteromeric GluN1/GluN2A/GluN2B NMDA receptors. *Neuron*. 81:1084–1096. https://doi.org/10.1016/j.neuron.2014.01.035
Hansen, K.B., L.P. Wollmuth, D. Bowie, H. Furukawa, F.S. Menniti, A.I. Sobolevsky, G.T. Swanson, S.A. Swanger, I.H. Greger, T. Nakagawa, et al. 2021. Structure, function, and pharmacology of glutamate receptor ion channels. *Pharmacol. Rev.* 73:298–487. https://doi.org/10.1124/pharmrev.120.000131
Helmstaedter, M., B. Sakmann, and D. Feldmeyer. 2009. Neuronal correlates of local, lateral, and translaminar inhibition with reference to cortical columns. *Cereb. Cortex*. 19:926–937. https://doi.org/10.1093/cercor/bhn141
Herring, B.E., and R.A. Nicoll. 2016. Long-term potentiation: From CaMKII to AMPA receptor trafficking. *Annu. Rev. Physiol.* 78:351–365. https://doi.org/10.1146/annurev-physiol-021014-071753
Hubalkova, P., M. Ladislav, V. Vyklicky, T. Smejkalova, B. Hrcka Krausova, B. Kysilov, J. Krusek, Z. Naimová, M. Korinek, H. Chodounska, et al. 2021. Palmitoylation controls NMDA receptor function and steroid sensitivity. *J. Neurosci.* 41:2119–2134. https://doi.org/10.1523/JNEUROSCI.2654-20.2021
Indurthi, D.C., and A. Auerbach. 2023. Agonist efficiency links binding and gating in a nicotinic receptor. *Elife*. 12:12. https://doi.org/10.7554/eLife.86496
Jackson, M.B., B.S. Wong, C.E. Morris, H. Lecar, and C.N. Christian. 1983. Successive openings of the same acetylcholine receptor channel are correlated in open time. *Biophys. J.* 42:109–114. https://doi.org/10.1016/S0006-3495(83)84375-6
Karakas, E., and H. Furukawa. 2014. Crystal structure of a heterotetrameric NMDA receptor ion channel. *Science*. 344:992–997. https://doi.org/10.1126/science.1251915
Kazi, R., J. Dai, C. Sweeney, H.X. Zhou, and L.P. Wollmuth. 2014. Mechanical coupling maintains the fidelity of NMDA receptor-mediated currents. *Nat. Neurosci.* 17:914–922. https://doi.org/10.1038/nn.3724
Kazi, R., Q. Gan, I. Talukder, M. Markowitz, C.L. Salussolia, and L.P. Wollmuth. 2013. Asynchronous movements prior to pore opening in NMDA receptors. *J. Neurosci.* 33:12052–12066. https://doi.org/10.1523/JNEUROSCI.5780-12.2013
Korinek, M., V. Vyklicky, J. Borovska, K. Lichnerova, M. Kaniakova, B. Krausova, J. Krusek, A. Balik, T. Smejkalova, M. Horak, and L. Vyklicky. 2015. Cholesterol modulates open probability and desensitization of NMDA receptors. *J. Physiol.* 593:2279–2293. https://doi.org/10.1113/jphysiol.2014.288209
Krupp, J.J., B. Vissel, C.G. Thomas, S.F. Heinemann, and G.L. Westbrook. 2002. Calcineurin acts via the C-terminus of NR2A to modulate desensitization of NMDA receptors. *Neuropharmacology*. 42:593–602. https://doi.org/10.1016/S0028-3908(02)00031-X
Lee, C.H., W. Lü, J.C. Michel, A. Goehring, J. Du, X. Song, and E. Gouaux. 2014. NMDA receptor structures reveal subunit arrangement and pore architecture. *Nature*. 511:191–197. https://doi.org/10.1038/nature13548
Legendre, P., C. Rosenmund, and G.L. Westbrook. 1993. Inactivation of NMDA channels in cultured hippocampal neurons by intracellular calcium. *J. Neurosci.* 13:674–684. https://doi.org/10.1523/JNEUROSCI.13-02-00674.1993
Lester, R.A., J.D. Clements, G.L. Westbrook, and C.E. Jahr. 1990. Channel kinetics determine the time course of NMDA receptor-mediated synaptic currents. *Nature*. 346:565–567. https://doi.org/10.1038/346565a0
Mainen, Z.F., R. Malinow, and K. Svoboda. 1999. Synaptic calcium transients in single spines indicate that NMDA receptors are not saturated. *Nature*. 399:151–155. https://doi.org/10.1038/20187
Maki, B.A., and G.K. Popescu. 2014. Extracellular Ca(2+) ions reduce NMDA receptor conductance and gating. *J. Gen. Physiol.* 144:379–392. https://doi.org/10.1085/jgp.201411244
McDaniel, M.J., K.K. Ogden, S.A. Kell, P.B. Burger, D.C. Liotta, and S.F. Traynelis. 2020. NMDA receptor channel gating control by the pre-M1 helix. *J. Gen. Physiol.* 152:152. https://doi.org/10.1085/jgp.201912362
Mony, L., and P. Paoletti. 2023. Mechanisms of NMDA receptor regulation. *Curr. Opin. Neurobiol.* 83:102815. https://doi.org/10.1016/j.conb.2023.102815
Murphy, J.A., I.S. Stein, C.G. Lau, R.T. Peixoto, T.K. Aman, N. Kaneko, K. Aromolaran, J.L. Saulnier, G.K. Popescu, B.L. Sabatini, et al. 2014. Phosphorylation of Ser1166 on GluN2B by PKA is critical to synaptic NMDA receptor function and Ca^{2+} signaling in spines. *J. Neurosci.* 34:869–879. https://doi.org/10.1523/JNEUROSCI.4538-13.2014
Nayak, T.K., R. Vij, I. Bruhova, J. Shandilya, and A. Auerbach. 2019. Efficiency measures the conversion of agonist binding energy into receptor conformational change. *J. Gen. Physiol.* 151:465–477. https://doi.org/10.1085/jgp.201812215
Ogden, K.K., W. Chen, S.A. Swanger, M.J. McDaniel, L.Z. Fan, C. Hu, A. Tankovic, H. Kusumoto, G.J. Kosobucki, A.J. Schulien, et al. 2017. Molecular mechanism of disease-associated mutations in the pre-M1 helix of NMDA receptors and potential rescue pharmacology. *PLoS Genet.* 13:e1006536. https://doi.org/10.1371/journal.pgen.1006536

Pampaloni, N.P., and A.J.R. Plested. 2022. Slow excitatory synaptic currents generated by AMPA receptors. *J. Physiol.* 600:217–232. https://doi.org/10.1113/JP280877

Pampaloni, N.P., I. Riva, A.L. Carbone, and A.J.R. Plested. 2021. Slow AMPA receptors in hippocampal principal cells. *Cell Rep.* 36:109496. https://doi.org/10.1016/j.celrep.2021.109496

Paoletti, P., C. Bellone, and Q. Zhou. 2013. NMDA receptor subunit diversity: Impact on receptor properties, synaptic plasticity and disease. *Nat. Rev. Neurosci.* 14:383–400. https://doi.org/10.1038/nrn3504

Popescu, G., and A. Auerbach. 2003. Modal gating of NMDA receptors and the shape of their synaptic response. *Nat. Neurosci.* 6:476–483. https://doi.org/10.1038/nn1044

Popescu, G., A. Robert, J.R. Howe, and A. Auerbach. 2004. Reaction mechanism determines NMDA receptor response to repetitive stimulation. *Nature.* 430:790–793. https://doi.org/10.1038/nature02775

Prüss, H. 2021. Autoantibodies in neurological disease. *Nat. Rev. Immunol.* 21:798–813. https://doi.org/10.1038/s41577-021-00543-w

Rauner, C., and G. Köhr. 2011. Triheteromeric NR1/NR2A/NR2B receptors constitute the major N-methyl-D-aspartate receptor population in adult hippocampal synapses. *J. Biol. Chem.* 286:7558–7566. https://doi.org/10.1074/jbc.M110.182600

Rosenmund, C., A. Feltz, and G.L. Westbrook. 1995. Synaptic NMDA receptor channels have a low open probability. *J. Neurosci.* 15:2788–2795. https://doi.org/10.1523/JNEUROSCI.15-04-02788.1995

Rosenmund, C., and G.L. Westbrook. 1993. Rundown of N-methyl-D-aspartate channels during whole-cell recording in rat hippocampal neurons: Role of Ca^{2+} and ATP. *J. Physiol.* 470:705–729. https://doi.org/10.1113/jphysiol.1993.sp019884

Salter M.W., Y. Dong, L.V. Kalia, X.J. Liu, and G. Pitcher. 2009. Regulation of NMDA receptors by kinases and phosphatases. *Nature.* 369:233–235. https://doi.org/10.1038/369233a0

Sheng, M., J. Cummings, L.A. Roldan, Y.N. Jan, and L.Y. Jan. 1994. Changing subunit composition of heteromeric NMDA receptors during development of rat cortex. *Nature.* 368:144–147. https://doi.org/10.1038/368144a0

Sun, W., K.B. Hansen, and C.E. Jahr. 2017. Allosteric interactions between NMDA receptor subunits shape the developmental shift in channel properties. *Neuron.* 94:58–64.e3. https://doi.org/10.1016/j.neuron.2017.03.018

Talukder, I., P. Borker, and L.P. Wollmuth. 2010. Specific sites within the ligand-binding domain and ion channel linkers modulate NMDA receptor gating. *J. Neurosci.* 30:11792–11804. https://doi.org/10.1523/JNEUROSCI.5382-09.2010

Tian, M., D. Stroebel, L. Piot, M. David, S. Ye, and P. Paoletti. 2021. GluN2A and GluN2B NMDA receptors use distinct allosteric routes. *Nat. Commun.* 12:4709. https://doi.org/10.1038/s41467-021-25058-9

Tovar, K.R., M.J. McGinley, and G.L. Westbrook. 2013. Triheteromeric NMDA receptors at hippocampal synapses. *J. Neurosci.* 33:9150–9160. https://doi.org/10.1523/JNEUROSCI.0829-13.2013

Traynelis, S.F., and S.G. Cull-Candy. 1991. Pharmacological properties and H+ sensitivity of excitatory amino acid receptor channels in rat cerebellar granule neurones. *J. Physiol.* 433:727–763. https://doi.org/10.1113/jphysiol.1991.sp018453

Traynelis, S.F., L.P. Wollmuth, C.J. McBain, F.S. Menniti, K.M. Vance, K.K. Ogden, K.B. Hansen, H. Yuan, S.J. Myers, and R. Dingledine. 2010. Glutamate receptor ion channels: Structure, regulation, and function. *Pharmacol. Rev.* 62:405–496. https://doi.org/10.1124/pr.109.002451

Vance, K.M., K.B. Hansen, and S.F. Traynelis. 2012. GluN1 splice variant control of GluN1/GluN2D NMDA receptors. *J. Physiol.* 590:3857–3875. https://doi.org/10.1113/jphysiol.2012.234062

Vance, K.M., K.B. Hansen, and S.F. Traynelis. 2013. Modal gating of GluN1/GluN2D NMDA receptors. *Neuropharmacology.* 71:184–190. https://doi.org/10.1016/j.neuropharm.2013.03.018

Vance, K.M., N. Simorowski, S.F. Traynelis, and H. Furukawa. 2011. Ligand-specific deactivation time course of GluN1/GluN2D NMDA receptors. *Nat. Commun.* 2:294. https://doi.org/10.1038/ncomms1295

Vyklicky, V., C. Stanley, C. Habrian, and E.Y. Isacoff. 2021. Conformational rearrangement of the NMDA receptor amino-terminal domain during activation and allosteric modulation. *Nat. Commun.* 12:2694. https://doi.org/10.1038/s41467-021-23024-z

Wang, H., S. Lv, D. Stroebel, J. Zhang, Y. Pan, X. Huang, X. Zhang, P. Paoletti, and S. Zhu. 2021. Gating mechanism and a modulatory niche of human GluN1-GluN2A NMDA receptors. *Neuron.* 109:2443–2456.e5. https://doi.org/10.1016/j.neuron.2021.05.031

Wang, J., F. Wang, D. Mai, and S. Qu. 2020. Molecular mechanisms of glutamate toxicity in Parkinson's disease. *Front. Neurosci.* 14:585584. https://doi.org/10.3389/fnins.2020.585584

Wang, Y.T., Y.S. Pak, and M.W. Salter. 1993. Rundown of NMDA-receptor mediated currents is resistant to lowering intracellular $[Ca^{2+}]$ and is prevented by ATP in rat spinal dorsal horn neurons. *Neurosci. Lett.* 157:183–186. https://doi.org/10.1016/0304-3940(93)90732-Z

Wang, Y.T., X.M. Yu, and M.W. Salter. 1996. Ca(2+)-independent reduction of N-methyl-D-aspartate channel activity by protein tyrosine phosphatase. *Proc. Natl. Acad. Sci. USA.* 93:1721–1725. https://doi.org/10.1073/pnas.93.4.1721

Watanabe, J., A. Rozov, and L.P. Wollmuth. 2005. Target-specific regulation of synaptic amplitudes in the neocortex. *J. Neurosci.* 25:1024–1033. https://doi.org/10.1523/JNEUROSCI.3951-04.2005

Watkins, J.C., and D.E. Jane. 2006. The glutamate story. *Br. J. Pharmacol.* 147:S100–S108. https://doi.org/10.1038/sj.bjp.0706444

Wollmuth, L.P., K. Chan, and L. Groc. 2021. The diverse and complex modes of action of anti-NMDA receptor autoantibodies. *Neuropharmacology.* 194:108624. https://doi.org/10.1016/j.neuropharm.2021.108624

XiangWei, W., Y. Jiang, and H. Yuan. 2018. De novo mutations and Rare variants occurring in NMDA receptors. *Curr. Opin. Physiol.* 2:27–35. https://doi.org/10.1016/j.cophys.2017.12.013

Yao, Y., J. Belcher, A.J. Berger, M.L. Mayer, and A.Y. Lau. 2013. Conformational analysis of NMDA receptor GluN1, GluN2, and GluN3 ligand-binding domains reveals subtype-specific characteristics. *Structure.* 21:1788–1799. https://doi.org/10.1016/j.str.2013.07.011

Yelshansky, M.V., A.I. Sobolevsky, C. Jatzke, and L.P. Wollmuth. 2004. Block of AMPA receptor desensitization by a point mutation outside the ligand-binding domain. *J. Neurosci.* 24:4728–4736. https://doi.org/10.1523/JNEUROSCI.0757-04.2004

Yovanno, R.A., T.H. Chou, S.J. Brantley, H. Furukawa, and A.Y. Lau. 2022. Excitatory and inhibitory D-serine binding to the NMDA receptor. *eLife.* 11:11. https://doi.org/10.7554/eLife.77645

Yu, A., and A.Y. Lau. 2018. Glutamate and Glycine binding to the NMDA receptor. *Structure.* 26:1035–1043.e2. https://doi.org/10.1016/j.str.2018.05.004

Zhang, J., M. Zhang, Q. Wang, H. Wen, Z. Liu, F. Wang, Y. Wang, F. Yao, N. Song, Z. Kou, et al. 2023. Distinct structure and gating mechanism in diverse NMDA receptors with GluN2C and GluN2D subunits. *Nat. Struct. Mol. Biol.* 30:629–639. https://doi.org/10.1038/s41594-023-00959-z